

DETERMINATION OF 3D GRAVITY SOURCE AND ITS DEPTH BENEATH CAMEROON VOLCANIC LINE (CVL) USING DEXP TRANSFORMATION

N. E. Ekolle*1, A. N. Vasilevskiy^{1,2}, and E. I. Esin^{1,2}

Abstract: The Cameroon Volcanic Line (CVL), which is around 1600 km long, the Adamawa Plateau, the northern sedimentary basins, the Central African Shear Zone, and the northern boundary between the Pan-African Mobile Belt and Congo Craton are the primary geological features of Cameroon. A good number of authors have attempted to comprehend the geology and gravity field along the CVL by using gravitational data from the EGM2008 model to analyze the gravity effects in areas around Cameroon and the CVL with a focus on its structures and subsurface characteristics. Despite the fact that many authors have written on the subject matter, more emphasis has to be placed on the determination of the gravity source and depth beneath the CVL. Experimental gravity field model XGM2019e_2159 and DTU21 data were used in this research to estimate the depth of the gravity source. Both DEXP (Depth from Extreme Points) and spectral analysis were carried out to complement the results and accuracy of the techniques. The main focus of this research is to investigate the gravity source depth of CVL using DEXP as the main approach to illustrate its application in solving geophysical and geologic problems and reveal details of volcanic structures beneath the CVL. In this work, we describe the steps taken to calculate the anomalous gravity field and regional and residual gravitational effects. We further performed application of the DEXP transformation of 3D gravity field distribution to produce a 3D model for the depth of gravity sources.

Keywords: Cameroon Volcanic Line, DEXP Transformation, 3D gravity model, Spectral Analysis, Structural index.

Citation: Ekolle, N. E., A. N. Vasilevskiy, and E. I. Esin (2025), Determination of 3D Gravity Source and Its Depth Beneath Cameroon Volcanic Line (CVL) Using DEXP Transformation, *Russian Journal of Earth Sciences*, 25, ES3011, EDN: ZLKZQK, https://doi.org/10.2205/2025es000991

RESEARCH ARTICLE

Received: 21 March 2024 Accepted: 21 January 2025 Published: 4 June 2025



Copyright: © 2025. The Authors. This article is an open access article distributed under the terms and conditions of the Creative Commons Attribution (CC BY) license (https://creativecommons.org/licenses/by/4.0/).

1. Introduction

Global Geopotential Model (GGM) system uses data from satellites, ground gravity measurements across different seas, and continental surface measurements from satellites over the oceans to recreate the gravity field of the Earth up to degree and order 2190 [Förste et al., 2014; Gilardoni et al., 2016; Pavlis et al., 2012]. Today, GGMs are useful options for synthesizing the Earth's gravitational field, particularly in regions lacking ground gravimetric measurements or where information is insufficiently covered [Abd-Elmotaal et al., 2018]. Because of sources that are either extremely large to be covered by the survey area or deeper enough to be easily seen on a regional or local gravity map, major anomalies are frequently concealed in a gravity field [Ghomsi et al., 2021].

Ground gravitational field characteristics derived from the EGM2008 model have been widely employed in geophysical and geodetic studies of Cameroon [Gautier Kamto et al., 2020]. For instance, [Abate Essi et al., 2017] employed gravity data from the EGM2008 model to analyze the subsurface of Central and Northern Cameroon with consequences

¹Novosibirsk State University, Novosibirsk, Russia

²Trofimuk Institute of Petroleum Geology and Geophysics (SB RAS), Novosibirsk, Russia

^{*} Correspondence to: Ndinde Eya Ekolle, ekolleeya@gmail.com; n.ekoll@alumni.nsu.ru

for mining and identify the geometric properties of Mamfe basin. By combining ground and satellite gravity data [Kamto et al., 2021] precisely characterize the southern coastline region of Cameroon.

According to [Moundi et al., 2007] and [Yokoyama et al., 2007], the Cameroon Volcanic Line (CVL), which consists of both continental and oceanic plates, has been erupting for 52 million years to this current time. The continental portion is distinguished by Mount Cameroon's volcanism and a fatal gas release from lakes Monoun and Nyos in 1984 and 1986, respectively, and the oceanic portion includes the Gulf of Guinea and Bioko Island as a hotspot [Marcel et al., 2018; Suh et al., 2003].

Many authors have attempted to comprehend the geology and gravity field along the CVL [Cheunteu Fantah et al., 2022; Kamgang et al., 2010; Kenfack et al., 2011; Ndikum et al., 2014; Njeudjang et al., 2020]. [Marcel et al., 2018] use gravitational data from the EGM2008 model to analyze the Cameroon Volcanic Line with a focus on its structure and subsurface characteristics. Also, further studies on the depth evaluation of CVL have been made by different researchers using gravity and seismic approaches. [Fairhead and Okereke, 1987] used gravity linear segments of the radially averaged power spectrum to calculate average depths to density discontinuities of 30 ± 3 km for the SW of Cameroon. Other studies have used spectral analysis to calculate the depth of the CVL from shallow and deep sources [Evariste et al., 2014; Kenfack et al., 2017; Marcel et al., 2016; Nnange et al., 2000]. Additional methods such as seismic Rayleigh waves [Tokam et al., 2010] and passive seismic [Goussi Ngalamo et al., 2018] have been used to calculate the Moho depth of CVL. Although, many authors have written on the subject matter, more emphasis needs to be placed on the determination of the gravity source and depth beneath the Cameroon Volcanic Line.

This work is aimed at constructing a 3D gravity model in order to calculate the depth and location of gravity sources beneath CVL starting from Bioko Island and including Mt. Cameroon, Mt. Kupe, Mt. Manengouba, Mt. Bambouto, and Mt. Oku by using data collected from a more precise and advanced Earth Gravitational Model (XGM2019e_2159). We also reveal the detailed geology of the study area.

2. Geologic Setting

The break-up of the continental plates can be interpreted in terms of an anticlockwise movement of the West Africa plate against the South America plate [Lawrence et al., 2002]. Cameroon is part of a complex that encompasses various tectonic formations, the Congo Craton, and a major geologic feature in Central Africa known as the Cameroon Volcanic Line [Dumont, 1986; Noel et al., 2014; Toteu et al., 2004].

CVL lies between the southern craton of the Congo and the northern craton of the Oubanguides, which was formed by the tectonic collision of four different cratons, which include the Congo, West Africa, São Francisco, and a mobile domain in the formation of Gondwana [Begg et al., 2009; Castaing et al., 1994; Elsheikh et al., 2014; Tokam et al., 2010].

There are three sections to the volcanoes along the Cameroon Line, which include a continental part made up of Mount Manengouba, Bambouto, and Oku; a middle portion that combines the continental-oceanic boundary, consisting of Bioko Island, Mt. Cameroon, Mount Etinde, and Mount Kupe; and lastly, an oceanic part made up of the islands of Pagalu, São Tomé, and Príncipe [Aka et al., 2004; Burke, 2001; Yokoyama et al., 2007].

The CVL's largest and most active volcano is Mount Cameroon (4095 m), which is made primarily of basaltic composition and situated where the lithospheres of the ocean and continent meet [*Déruelle et al.*, 2007; *Kenfack et al.*, 2011]. The plutonic structures are separated in the north and combine to form composite structures between Banyo and Foumban [*Njome and de Wit*, 2014].

The research area (Figure 1), which is a portion of the CVL, is located at latitudes 3°50′ and 6°50′N and longitudes 8°50′ and 12°00′E.

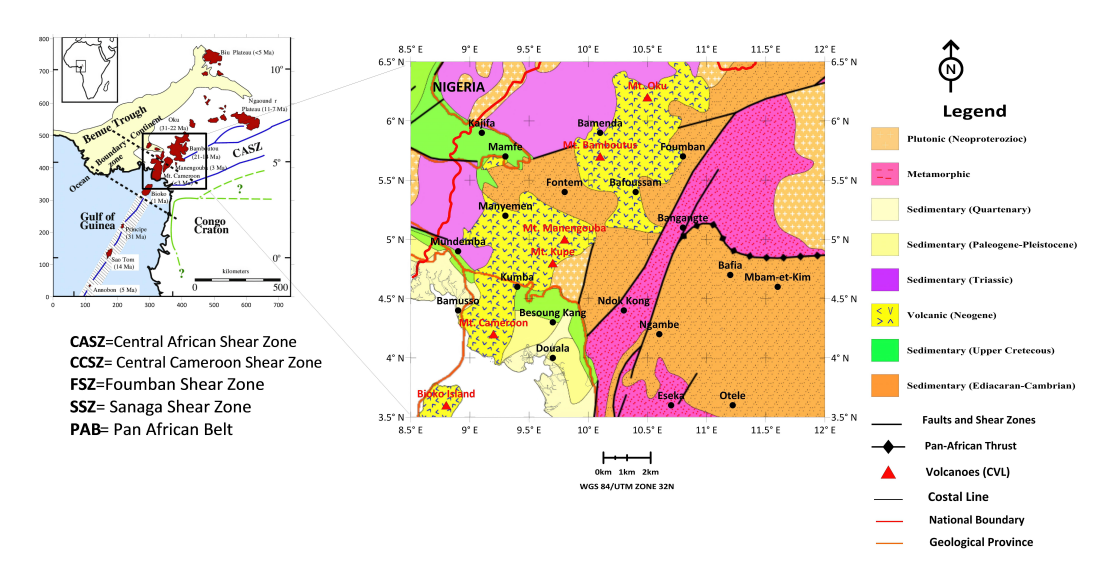


Figure 1. Region of investigations: Geology and Tectonic Map of CVL.

3. Data and Methods

3.1. Data

The International Center for Global Earth Models (ICGEM) website (http://icgem.gfz-potsdam.de/home) was used to download the required data. Free air gravity data from XGM2019e_2159 and the DTU21 model was used in this research for depth estimation of the CVL. The ICGEM compiles the spherical harmonic coefficients of all Global Geopotential Models (GGMs) [Barthelmes, 2013] that is available for download. ICGEM is one of the services run by IGFS (International Gravity Field Service) [Drewes et al., 2016]. The satellite-based Global Geopotential Model (GGM) known as GOCO06S was integrated with terrestrial and altimetry data used for modeling XGM2016 to create XGM2019e_2159 [Lee and Kwon, 2020].

According to [*Lee and Kwon*, 2020], gravity data from satellites can be accessed in locations that are difficult to get to on the ground and solve the problem of gaps and low resolutions obtained from ground gravity data. Several researchers have supported the use of this gravity database by comparing their results with those derived from different sources of geophysical data [*Apeh and Tenzer*, 2022; *Gruber et al.*, 2019; *Zingerle et al.*, 2019].

In this research Free air and Bouguer anomaly maps were created using gravity data that was downloaded from ICGEM. The grid size was chosen before carrying out the online computations of XGM2019e_2159 free air (Figure 3) and Bouguer gravity data (Figure 4) using the ICGEM service. The gridding technique provides an interpolated surface that can be compared to a tiny, linear elastic layer that passes over each value of the data with the lowest number of bindings possible [Marcel et al., 2018].

Topographic data was obtained using the same latitude and longitude values from the global database (Global Multi-Resolution Topography) through the website (https://www.gmrt.org/GMRTMapTool/). Golden Software Surfer was also used to create the topographic map (Figure 2) of the Cameroon Volcanic Line, with a maximum height of 4000 meters above sea level. Using a unique function of spherical approximation (option gravity_anomaly_sa), gravity data for different heights to be used in 3D models was carefully acquired from the ICGEM website.

3.1.1. Free Air Gravity Anomaly

The Free Air gravity anomaly (Figure 3) shows a maximum gravity anomaly of $530\,\mathrm{mGal}$ and a minimum of $-100\,\mathrm{mGal}$. The main zones of high gravity values are found along the volcanoes of the CVL, which have a higher elevation than the surrounding rock masses. The Free Air anomaly was used for the determination of the depth of the gravity source using the DEXP method.

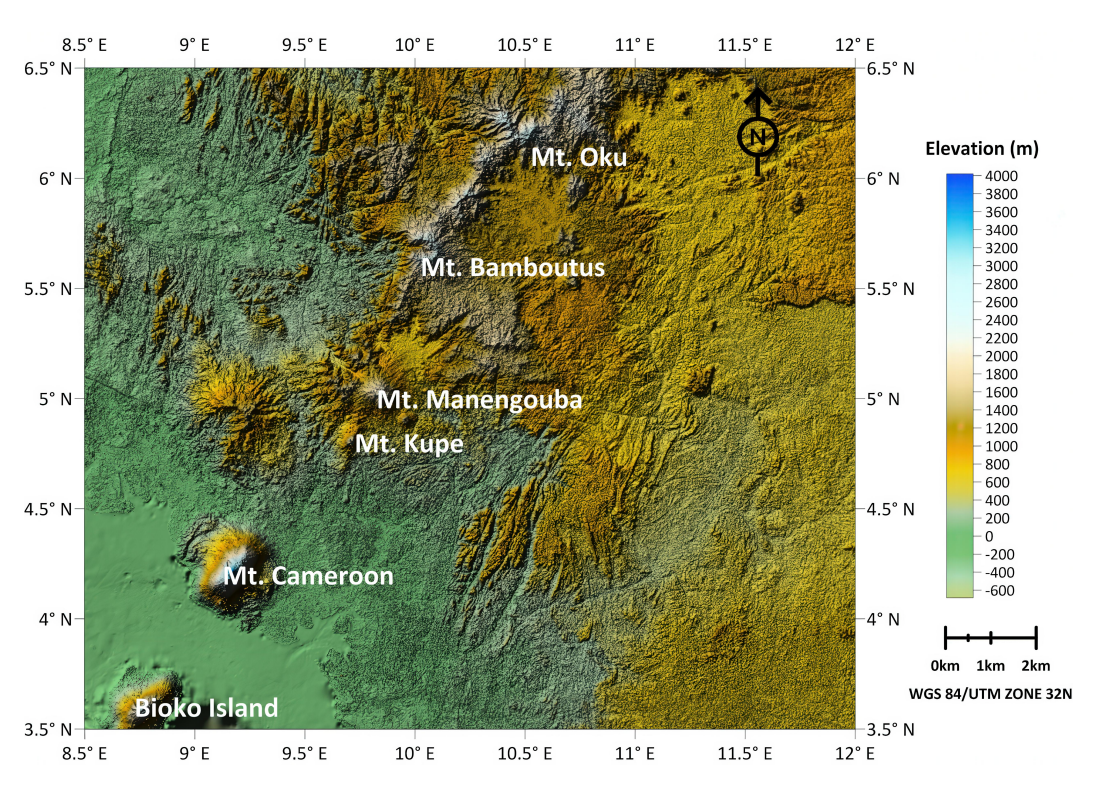


Figure 2. Topographic Map of the study area in the Cameroon Volcanic Line.

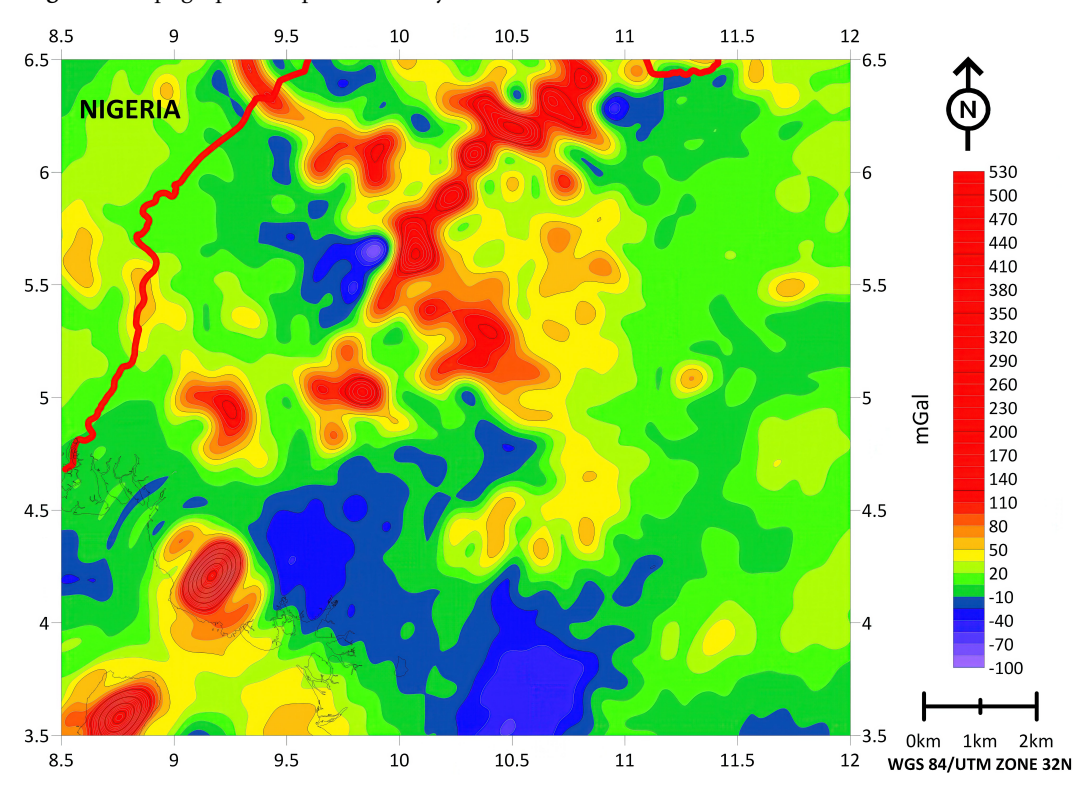


Figure 3. Free Air gravity anomaly of the study area.

3.1.2. Bouguer Anomalies and Residual Bouguer Anomalies

The study area's Bouguer anomaly map (Figure 4) was gridded using the WGS84 reference system, with a required angular grid spacing of 0.02°. The map was then created with a contour interval of 10 mGal. The research area is distinguished by significantly high positive anomaly values, particularly in the West and South West portions, with a

9.5° F 8.5° F 9° F 10° E 10.5° E 11.5° E 12° E 11° E 6.5° N 6.5° N Mt. Oku **NIGERIA** 6° N Kajifa 6° N mGal Mt. Bamboutus Mamfe 180 160 140 5.5° N **Bafoussam** 5.5° N ontem 120 Manyemen 100 Bangangt 80 60 5° N 5° N Mundemba 40 20 Mbam-et-Kim 0 Kumba -20 4.5° N 4 5° N **Bamusso Ndok Kong** -40 **Besoung Kang** -60 Ngambe -80 -100 Douala 4° N 4° N -120 -140 Bioko Island 0km 1km 2km 3 5° N 3 5° N WGS 84/UTM ZONE 32N 9° E 9.5° E 8.5° F 10° E 10.5° E 11° E 11.5° F 12° E

maximum of $200 \, \text{mGal}$ and a large area in the North and North East with a wide area of negative gravity anomaly values, with the lowest value being $-140 \, \text{mGal}$.

Figure 4. Bouguer anomaly map of the study area.

The study area's residual anomaly map (Figure 5) reveals interesting, specific geological features. The values of the residual gravity anomaly range from -80 to $180\,\mathrm{mGal}$. By creating the residual anomaly field from the measured gravity field, it is possible to determine the various gravity sources beneath the study area.

This residual anomaly field is produced by removing the regional anomaly from the Bouguer anomaly field. This process highlights sources located at very high depths because of long-wavelength anomalies on a regional scale across the entire area. Sources that are highly concentrated and localized with short wavelengths are typically found at shallow depths of the residual field [Abdelrahman et al., 1985; Murthy and Krishnamacharyulu, 1990; Ndikum et al., 2014].

Since both shallow and deep features in the Earth's subsurface have an effect, these effects cause Bouguer anomalies to have a gravitational signature. As residual anomalies offer a variety of lithology that is characterized by density fluctuations within the Earth's crust.

3.1.3. DTU21 Data

DTU21 data was provided by Professor Ole Baltazar Andersen (https://ftp.space.dtu.dk/pub/) in ASCII grid format. The map was produced with a grid spacing of 5 mGal. The DTU map (Figure 6) shows a high positive gravity anomaly in the mountain areas and a negative anomaly towards the south of the study area. The gravity anomaly in the study area ranges from -80 to 505 mGal.

3.2. Methods

Here, we will describe the steps taken to calculate the anomalous gravity field and regional and residual gravitational effects, including the creation of a gravity model, calculating the gravity field at various heights, formulation, and application of the DEXP transformation to 3D distribution. We also use several key methods, such as **spectral analysis**, **depth from the extreme points**, **and a 3D model**, to produce our results, and from these we carry out interpretations.

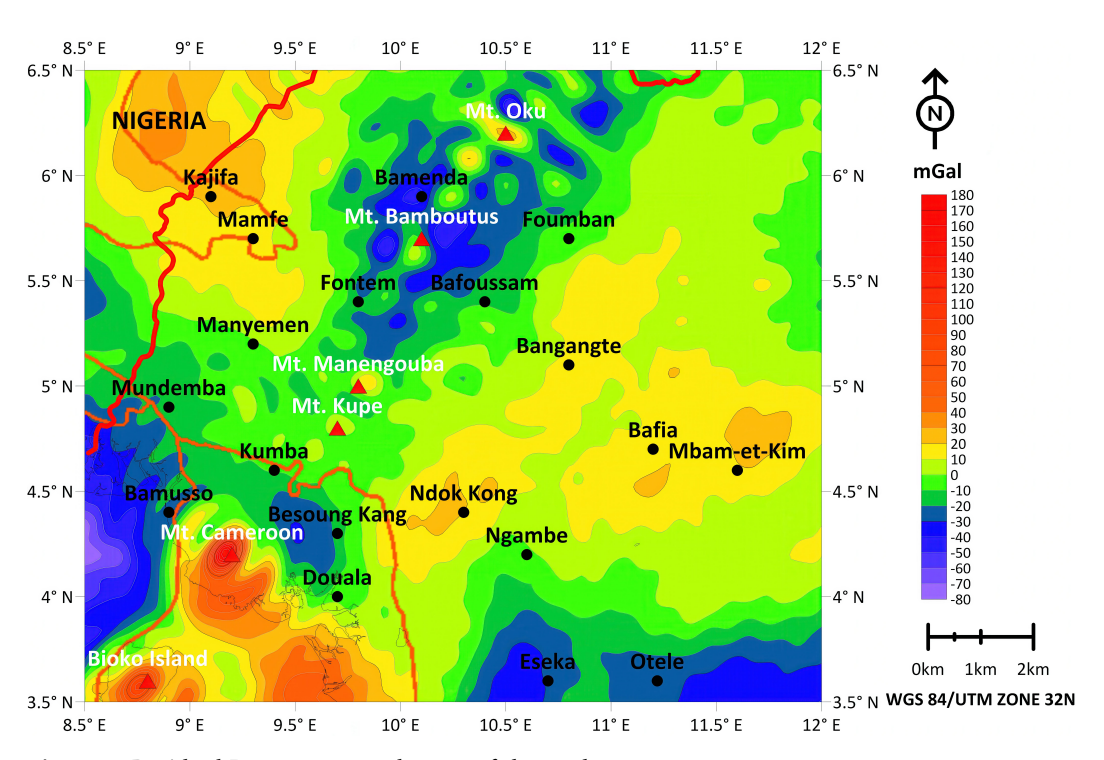


Figure 5. Residual Bouguer anomaly map of the study area.

With the use of the primary 15' NGA terrestrial gravity dataset, the GOCO06s satellite gravity model are adjusted using weighted least squares to determine the XGM2019 spheroidal harmonic model coefficients up to d/o 719 [Zingerle et al., 2019]. We used a specified grid size of 0.01° and data for ellipsoid topographic heights at various elevations of the study site, and the anomalous gravity values were calculated online through the ICGEM website platform. A similar technique was used by [Drewes et al., 2016] and [Apeh and Tenzer, 2022].

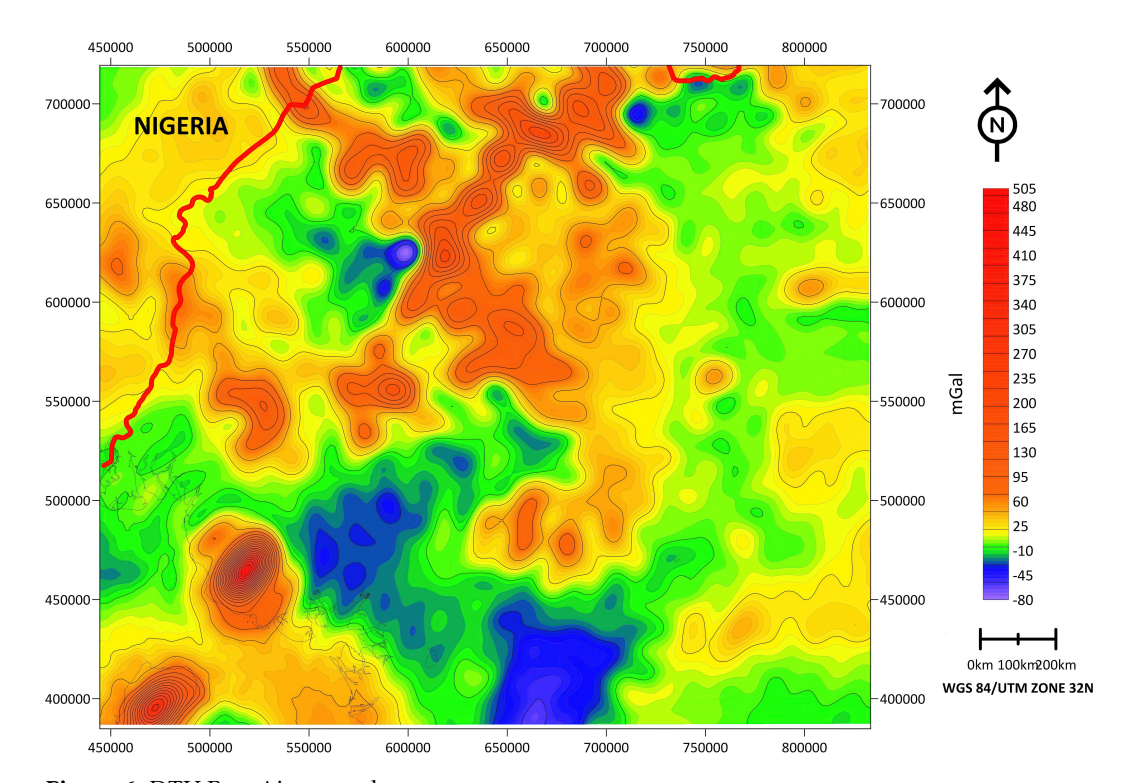


Figure 6. DTU Free Air anomaly map.

By computing the function of the polynomial regression method [Draper and Smith, 1998; Gautier Kamto et al., 2020; Ghomsi et al., 2021; Murthy and Krishnamacharyulu, 1990] and Kriging using Golden Software Surfer, the regional Bouguer and residual Bouguer anomaly maps were produced, respectively. Prediction errors are reduced by using the Kriging interpolation approach [Gautier et al., 2021], and it is possible to identify biased values using the technique of Kriging [Kamguia et al., 2007; Matheron, 1963]. We have applied a second-order polynomial regression on the XGM2019e_2159 model grid because we wanted to avoid eliminating shallow structures represented in the residual anomalies. This was accomplished by using a polynomial (regression) fitting method similar to that employed by [Gautier Kamto et al., 2020; Ghomsi et al., 2021], which enables the division of Bouguer anomalies into regional and residual parts.

3.2.1. Spectral Analysis

Spectral analysis is a method often used by scientists to find out how deeply certain properties of a medium are related to the gravitational field [Marcel et al., 2010; Njandjock et al., 2006; Spector and Grant, 1970]. This process involves the transformation of gravitational data from the spatial domain to the wavenumber domain using a 2-dimensional Fourier transform [Nnange et al., 2000]. [Spector and Grant, 1970] showed that the Fourier transform for a set of N data points spread out over a profile can be used to find out the depth of the sources.

$$\Gamma(k) = \frac{1}{N} \sum_{n=0}^{N-1} R(n) e^{-\frac{2j\pi kn}{N}},$$

where R(n) – residual anomaly number n on the profile; k – wave number. The power spectrum of the anomaly – $|\Gamma(k)|^2$.

The energy spectrum logarithm is plotted against the frequency. The logarithm represents the radial average energy spectrum. The slope indicates the depth of gravity or a magnetic source.

Power spectrum curve can be broken down into many sections. These sections ties to the estimated depth of causative anomalies in the bodies of the geologic structure of a place [Nguiya et al., 2019]. We pick the straight lines that have a slope that's equal to the depth of the anomalous body based on this relationship [Gerard and Debeglia, 1975]:

$$h = \frac{\Delta \log E}{4\pi \Delta k},$$

where, E – energy spectrum; h – depth (km); k – wavelength (cycles per km).

Spectral analysis was carried out on DTU21 grid data over the whole study area to determined mean deep and shallow sources. Spectral analysis for DTU21 was performed based on **Wiener filtering** by distinguishing the gravity anomaly correlated with topography [Kokoshkin et al., 2015]. To filter the useful part of the field, it is necessary to know the spectrum of the full field and the spectrum of the field of the conceptual model, which we can obtain by calculating the gravitational field due to the relief of the day surface for a given relief density. This will restore the value of the approximation of the real and imaginary parts of the continuous spectrum in any given frequency range. Measurements of the influence of gravity on the path can be defined as [Zhou and Wu, 2015]:

$$y(t) = s(t) + v(t),$$

where s(t) – actual gravity signal; v(t) – colored noise between observations.

To improve our accuracy of deep source (Moho depth) estimation of the study area, we used the field separation procedure using **Wiener filtering** [*Esin et al.*, 2024]:

$$F_{v}(i,j) = \frac{|U_{os}(i,j)|^{2} F_{s}(i,j)}{|U_{os}(i,j)|^{2} + (|F_{s}(i,j)| - |U_{os}(i,j)|)^{2}}$$
(1)

where,

Signal spectrum:

 $F_s(i,j)$ – of original gravity field (DTU21 model)

 $F_v(i,j)$ – of restored signal that correlates with topography

Power spectrum:

 $|F_s(i,j)|^2$ – of original gravity signal

 $|U_{os}(i,j)|^2$ – of conceptual model of topography gravity field

3.2.2. DEXP Method

This method of field transformation appeared relatively recently [Fedi, 2007]. DEXP (depth from extreme points), allows one to achieve estimates of the depths of singular points of anomalous bodies, distributed in space under the area of setting the field values through express processing of the field. This is one of the simplest inversion algorithms, but it requires knowledge of the 3D field distribution to work.

This type of express inversion is used for potential fields (gravitational or magnetic) or its vertical derivatives of degree *n*:

$$f_n(\mathbf{r}) = k \int_V \frac{\partial^n}{\partial z^n} \frac{M(\mathbf{r}_0)}{\|\mathbf{r} - \mathbf{r}_0\|_2} d^3 \mathbf{r}_0,$$

where, $f_n(\mathbf{r})$ is the potential field or its vertical derivative (depending on n), k is some constant (gravitational constant), $M(\mathbf{r}_0)$ is the density, the integration is performed over the volume V, \mathbf{r} and \mathbf{r}_0 are spatial radius vectors connecting the origin of coordinates with a measurement point in the harmonic region and with some point in the source region.

First, let's introduce the concept of a structural index. In geophysics, this term is used as a determinant of the degree of a homogeneous function characteristic of magnetic or gravity prospecting – a homogeneous function of degree N:

$$f(x,y,z) = \frac{K}{r^N},$$

$$r = \left(x^2 + y^2 + z^2\right)^{\frac{1}{2}}$$

where, N = 1, 2, 3..., K = const.

Moreover, a homogeneous function is called when the following relation is fulfilled:

$$f(tx,ty,tz)=t^N\cdot f(x,y,z).$$

For this function, the following Euler equation is valid:

$$x\frac{\partial f}{\partial x} + y\frac{\partial f}{\partial y} + z\frac{\partial f}{\partial z} = Nf.$$

This equation can be used to localize gravitational and magnetic anomalies (it is important that all reasoning is given for "sliding windows" – some spatial constraints, inside of which operations are performed on the field). If we denote the interpreted function as U and assume that within the window its behavior can be explained by the nearest singular point - whose coordinates are x_0 , y_0 , z_0 . Then Euler's equation can be rewritten [*Bloch*, 2009]:

$$(x-x_0)\frac{\partial U(x,y,z)}{\partial x} + (y-y_0)\frac{\partial U(x,y,z)}{\partial y} + (z-z_0)\frac{\partial U(x,y,z)}{\partial z} = N[F-U(x,y,z)].$$

F – Constant regional background, N – structural index (where N corresponds to the degree of homogeneous function – N).

Thus, structural index is related to the extent of attenuation of the field of a studied source, which, in turn, is determined by the type of the sought-for feature and the type of the source.

In the DEXP method, the structural index plays a very important role, to understand which it is necessary to provide some considerations. First, consider a function of the form [Fedi, 2007]:

$$\tau_n(z) = \frac{\partial \log[f(z)]}{\partial \log(z)} = -\frac{(n+1)z}{z-z_0}.$$

It has one interesting property: for $z = -z_0$ (the coordinate of the singular point) – this function will take on a constant value depending only on n (n is the order of the derivative, it should be assumed that for n = 1 the field itself is considered, for n = 2 its derivative with respect to z):

$$\tau_n = -(n+1)/2.$$

In this research, we applied the Free Air gravity anomaly data of the XGM2019e_2159 model. By scaling a 3D field at extreme points using Surfer and Voxler software in accordance with certain power laws of the altitude, the DEXP approach enabled us to determine sources of anomalous bodies, depths, and the correct structural indexes. The positions of scaled fields' extreme points are used to determine the depths of sources, and their values are used to determine the surplus mass. This can facilitate pre-filtering, the reduction of reciprocal interference effects, and the acquisition of important representations of the allocation of sources vs. depth [Fedi, 2007]. We employ the well-known direct link between N and z_0 to compute the depth to the gravity source using DEXP technique [Fedi and Florio, 2013].

In order to apply the DEXP transformation, the upward continuation height of the Free Air anomaly was calculated and downloaded from the ICGEM website. The same geographical boundaries of latitude and longitude of the study area were chosen, and a grid step of 0.01° was selected. The heights were set online as heights over an ellipsoid in meters. The height for calculations of the gravitational fields was chosen from 1000 meters to 50000 meters.

The DEXP transformation is done by using a structural index (N) of 2 and 3. The structural index of 2 represents the field derivative, and 3 represents the second derivative. The structural index was chosen with the purpose of highlighting subsurface gravity sources and their depths, but it does not have a clear distribution of lineaments in the study area. [Fedi, 2007] states that after N is determined, the DEXP transformation is provided by:

$$W_n(Z) = Z^{\alpha_n} f_n(Z), \qquad S_n = 2\alpha_n, \tag{2}$$

where W_n – scaled field, f_n – array of field data, α_n – an exponent depending on the structural index, S_n – structural index, Z-DEXP power law of altitudes

$$S_n = 2\alpha_n = -2\tau_n \ (z = -z_0).$$

As a result of this scaling, you get a transformed field that has a bell-shaped shape. In the works of [Fedi, 2007], it is shown that this transformed field has extrema, the height of which mirrors the depth of the singular points of the anomaly-forming bodies. The DEXP inversion allows one to determine the position of singular points in space from the 3D distribution of the field, but to do this, it is necessary to know the correct values of α_n or S_n . The following is a table showing different types of sources, the structural index S_n and the scaling exponent α_n (Table 1).

We used a power of α_n = 1 to compute a transform field for structural index 2 and α_n = 1.5 for structural index 3.

Source type	Source	α_n , $(n=1)$	α_n , $(n=2)$	α_n , $(n=3)$	α_n , (n)	α_n , $(n=1)$	α_n , $(n=2)$	α_n , $(n=3)$
A	Point mass or dipole sources, spheres	1	1.5	2	$\alpha_n = 0.5(n+1)$	2	3	4
В	Line or masses or dipoles, infinite horizontal and vertical cylinder, thin bottomless prism	0.5	1	1.5	$\alpha_n = 0.5n$	1	2	3
С	Semi-infinite plane, thin dike, sill	(0)	0.5	1	$\alpha_n = 0.5(n-1),$ $n \le 1$	0	1	2
D	Semi-infinite contact	(-0.5)	0	0.5	$\alpha_n = 0.5(n-2),$ $n \le 2$	-1	0	1

Table 1. Structural indices and scale exponents for different types of sources and field derivatives [*Fedi*, 2007]

The DEXP transformation can be interpreted as a more general transformation that can be applied to any n-degree vertical derivative of a Newtonian pole source potential;

$$f_n(Z) = \frac{1}{(Z - Z_0)^{n+1}}. (3)$$

For example: By making calculations of equation (3) and (2) we can obtain the **depth** of a point source at -5 km by using the field derivative with a power of 2. We understand that:

Gravity field f above singular point decrease with altitude Z as

$$f_n(Z) \sim \frac{1}{(Z - Z_0)^{n+1}}.$$

Gravity field f above horizontal or vertical cylinder decrease with altitude Z as

$$f_n(Z) \sim \frac{1}{(Z-Z_0)^n},$$

where **n** – the degree of the derivative of the Newtonian potential, **n** = 1,2, **Z**₀ – **singular point** (source) depth, **Let** $\mathbf{Z}^{\alpha_{\mathbf{n}}}$ – scaling function α_n – **an exponent depending on the structural index**, α_n = 0.5(n + 1) – Point mass or dipole sources, spheres, α_n = 0.5n – Infinite horizontal and vertical cylinder, $\mathbf{S}_{\mathbf{n}}$ – structural index, $\mathbf{S}_{\mathbf{n}}$ = 2 α_n , $\mathbf{S}_{\mathbf{n}}$ = 1,2,3 [Fedi, 2007] states that scaled potential field

$$W_n(Z)=Z^{\alpha_n}f_n(Z)$$

It's a non-monotonic function and has an extremum at the altitude

$$Z = Z_{\text{extr}}$$

If true structure index of the gravity field is known it is easy to reveal z_0 by finding extremum of the scaled gravity $W_n(Z)$:

$$Z_0 = -Z_{\text{extr}}$$

Therefore, calculation of a Point source (sphere), where n = 1, $S_n = 2$. Get extremum at altitude 5 km. The depth to source \mathbf{Z}_0 will be -5 km. The following graph represents this extreme point. \mathbf{Z}_0 is the depth of gravity source beneath the Earth's crust, which can be referred to as negative height.

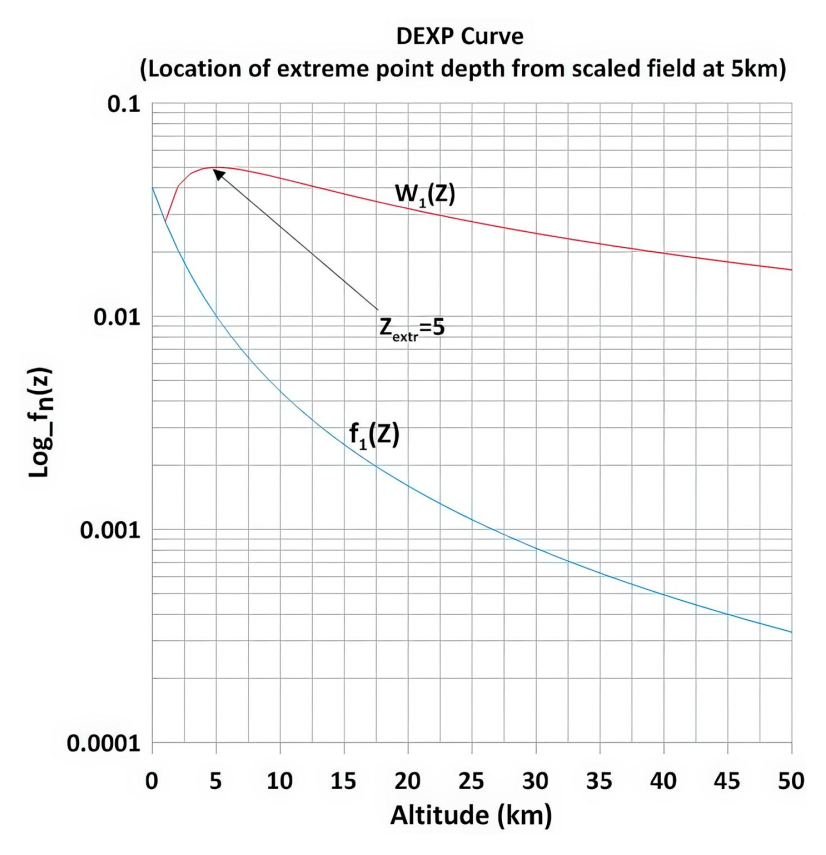


Figure 7. Location of extreme point depth from scaled field at 5 km.

At $x = x_0$ and $y = y_0$; the function $\log f_1 + \log z$; on the surface $\log[f_1(z, z_0)] + \log(z)$, we can see that, for any point at any depth of Z_0 , we have a curve with an extreme point at $-Z_0$.

The negative heights of gravity field extremes were calculated from the positive heights calculated from the ICGEM website to obtain the depth of gravity sources using Golden Software Surfer. Since it is important to obtain the results as depth measured in meters, the coordinates *X* and *Y*, which represent latitude and longitude, were transformed into meters using the coordinate system of the study area (Manoca 1962/UTM Zone 32N). Table 2 and Table 3 show sections of the data transformation sheet.

Depth of the source is estimated by the negative extreme point heights, and DEXP principle demonstrates that the extreme in the resulting function W_n relates to the location of the gravity source [Fedi, 2007; Fedi and Pilkington, 2011].

3.2.3. 3D Modeling

The gravity field anomaly obtained was successfully used to carry out 3D modeling of CVL. The aim was to visualize the gravity sources located deep beneath the CVL. The 3D field will be scaled in accordance with equation (2). When mapping the DEXP-transformed field W_n with regard to the \mathbf{Z}_0 axis in the DEXP-transformed field, the connection $\mathbf{Z}_0 = -Z_0$ was used (by adjusting the vertical axis to the depth of the sources). The transformed (scaled) field W_n makes it possible to find the depth when a height occurs at the right source point. Alternatively, by only inspecting the extreme points of W_n , the proper scaling of field vs. depth is sufficient to reveal the depth of the source of the potential field [Fedi, 2007].

The modeling was done with the help of Golden Software Voxler 4. In the modeling phase, the structural index values were calculated along a positive and negative anomalous gravity that produced a 3D model for the depth of gravity sources beneath CVL. The Z value in Voxler is the positive and negative directions or height (0 to 50 km and 0 to -50 km)

Table 2. Field derivative data structural index transformation

Longitude	Latitude	Gravity_anomaly_sa	Н	Н-	$\alpha_n = 1$	X	Y
8.50	6.5	-0.598999186436	0	0	0	444.85581	718.54653
8.51	6.5	-1.281784914657	0	0	0	445.96149	718.54545
8.52	6.5	-1.592648900128	0	0	0	447.06718	718.54439
8.53	6.5	-1.529360167163	0	0	0	448.17286	718.54336
8.54	6.5	-1.128670837377	0	0	0	449.27854	718.54234
8.55	6.5	-0.462289502852	0	0	0	450.38422	718.54135
8.56	6.5	0.371656055135	0	0	0	451.48990	718.54037
8.57	6.5	1.260665257675	0	0	0	452.59558	718.53942
8.58	6.5	2.091942859883	0	0	0	453.70125	718.53849
8.59	6.5	2.766737402928	0	0	0	454.80693	718.53759
8.60	6.5	3.213098266248	0	0	0	455.91260	718.53670
8.61	6.5	3.395376655234	0	0	0	457.01827	718.53584
8.62	6.5	3.319183209407	0	0	0	458.12394	718.53500
8.63	6.5	3.031076492912	0	0	0	459.22961	718.53418

Table 3. Second derivative structural index transformed field

Longitude	Latitude	Second_r_derivative	Н	Н-	$\alpha_n = 1.5$	X	Y
8.50	6.5	-20.612843501959	0	0	0	444.855806	718.546535
8.51	6.5	-21.791441167423	0	0	0	445.961492	718.545453
8.52	6.5	-21.865456174735	0	0	0	447.067177	718.544394
8.53	6.5	-20.833191241717	0	0	0	448.17286	718.543356
8.54	6.5	-18.824194409862	0	0	0	449.278541	718.542340
8.55	6.5	-16.085987461047	0	0	0	450.384221	718.541346
8.56	6.5	-12.955470442050	0	0	0	451.489900	718.540373
8.57	6.5	-9.8183019231600	0	0	0	452.595577	718.539423
8.58	6.5	-7.0611812071370	0	0	0	453.701253	718.538494
8.59	6.5	-5.0229829003100	0	0	0	454.806927	718.537587
8.60	6.5	-3.9509707922370	0	0	0	455.912600	718.536703
8.61	6.5	-3.9677960780900	0	0	0	457.018272	718.535840
8.62	6.5	-5.0537166314370	0	0	0	458.123942	718.534998
8.63	6.5	-7.0466092204260	0	0	0	459.2296111	718.534179

of the gravity sources of the CVL. The model consists of different shapes with a structural index (N) of 2 (Figure 8a) and 3 (Figure 8b) for each major point of the CVL. The local shapes represent the anomalous body.

The extent of a certain source is determined by *N*. In the works of [Fedi, 2007; Fedi and Pilkington, 2011; Fedi and Florio, 2013], it is shown that this transformed field has extremes, the height of which mirrors the depth of the singular points of the anomaly-forming bodies.

4. Results and Discussions

4.1. DEXP Results

The 3D gravity model displayed several depths of sources across CVL, with a maximum depth of 50 km, as shown in Figure 8 and 3D model of Geology Figure 9. The main gravity signatures found in the 3D model are of great interest for making remarks. CVL has different depth sources, as shown by the 3D model. Additionally, we observe

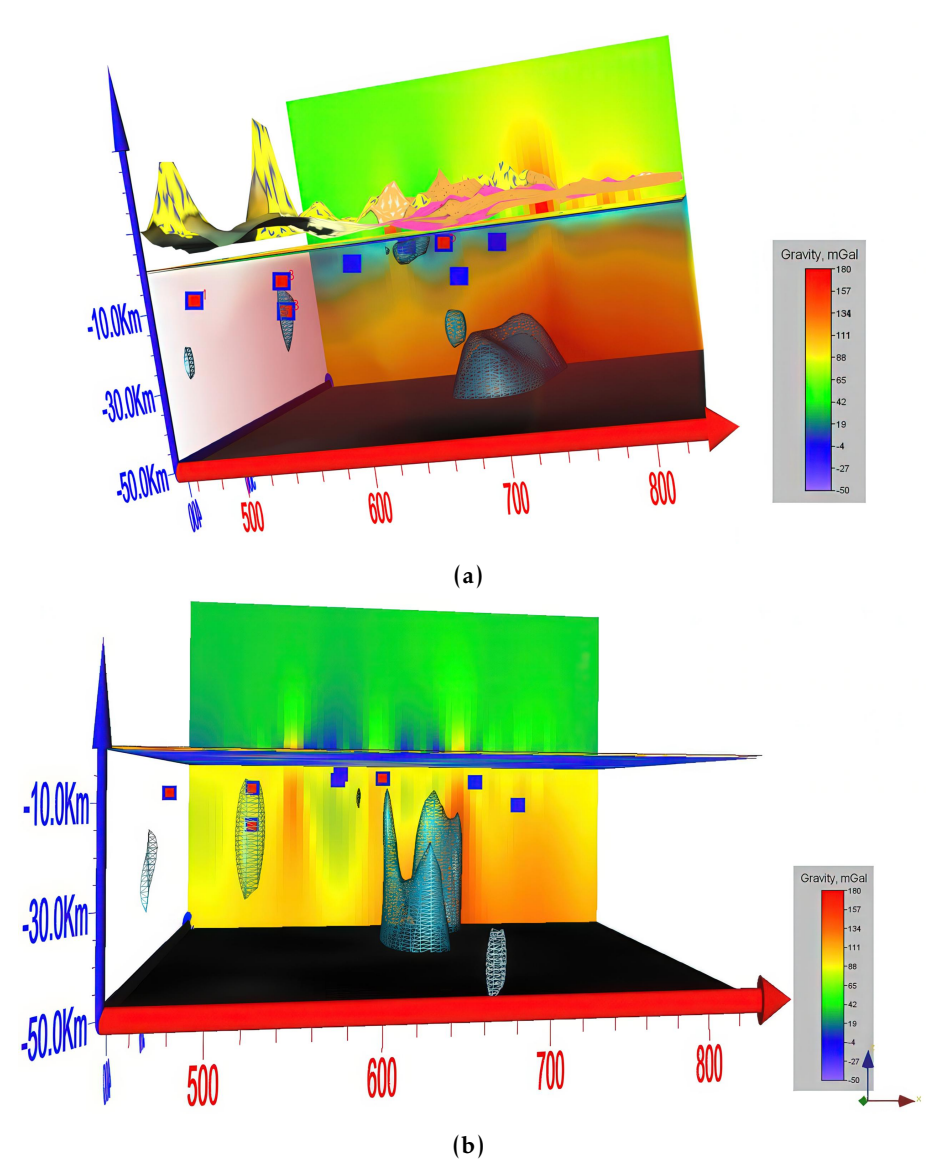


Figure 8. a) Free air gravity field DEXP transformation; b) Vertical derivative gravity field DEXP transformation.

that density anomalies of Bioko Island have gravity field sources at a depth of 8 km, and Mount Cameroon has a gravity field source depth of 7–12 km. This might be a result of the mountain being underlain by shallowly buried volcanic materials. A depth source is located 4–6 kilometers around the Manyemen and Fontem areas and 8–10 kilometers in the Douala Basin (Eséka). This may have been caused by the large area and thick deposition of sedimentary formations in the upper crust. Meanwhile, there is a deeper source depth of more than 30 km aligning to the north of the CVL from Mount Bamboutos to Mount Oku. Such a large difference in anomalous depth could either be a result of deep-seated igneous bodies found in the area. Deep singular points of the gravity field have revealed a true correlation with singular points of the gravity vertical gradient in the CVL.

It is important to make a comparison between our current research results and the depths of the gravity source in the studied area, as mentioned earlier. Research from [Marcel et al., 2016] presents a detailed study of shallow sources. The comparison (Table 5) presents a summarized study of four articles and estimated gravity source depths that were carried out in our area of interest by different authors using the spectral analysis method and the gravity source depth value obtained from DEXP, which was obtained from this research.

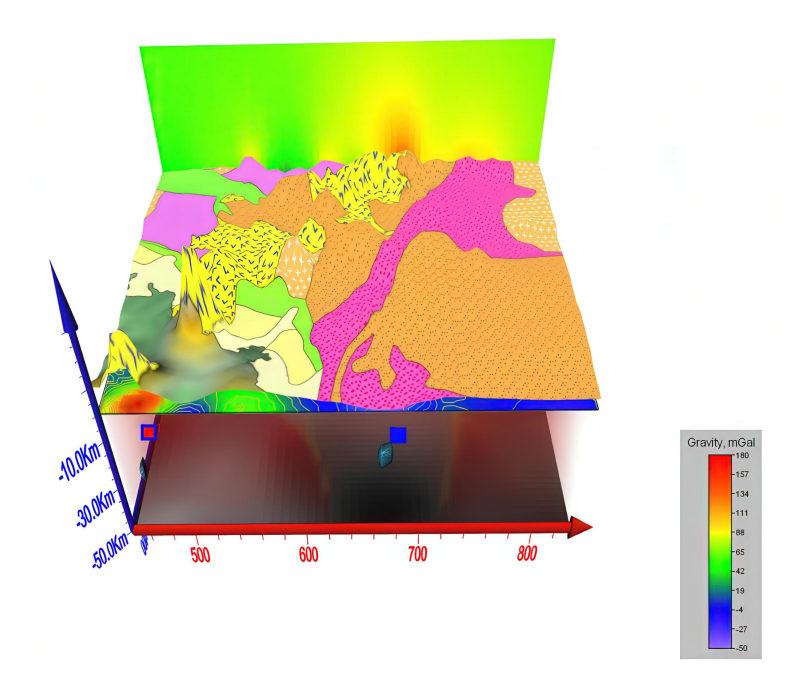


Figure 9. 3D model of geology and gravity field.

Table 4. Gravity Depth Estimate [Marcel et al., 2016]

Location (Anomalies)	Amplitude	Anomalies	Depth of shallow structures (km)	Shallow structure depth from previous studies (km)
Mount Cameroon, Limbe, (P1)	High	Positive	8–12	7–9
Kumba, (P2)	_	Negative	5–9	_
Manyemen, (P3)	High	Negative	4–8	4.5–7
Fontem, (P4)	High	Negative	6–8	4.5–7
Bafoussam, (NE Mt Cameroon), (P5)	-	Line of successive negative and positive superficial anomalies	5–9	-
NE Kumbo, (P6)	-	Line of successive negative and positive superficial anomalies	3–7	-
Ngambé, (P7)	High	Positive	5–7	-
Eséka, Makak, (P8)	-	Relatively negative anomalies	6–8	-

The table above represents the research results carried out by [Marcel et al., 2016]. The study represents a quite different approach to gravity depth estimations compared to the DEXP method. The shallowest layer has an estimated depth of 8 km. Other estimates range from 12 ± 2 km to 13 ± 2 km and 7 km. This could be because of the short-wavelength structures found in the area, which are linked to the volcanism in the Cameroon Line [Nnange et al., 2000].

Kenfack et al. [2017] found new depths in Mount Cameroon of 0.41 km, 1.26 km and 4.73 km. These new depths could be interpreted as the average depths of the sources that cause the negative anomalies at the mountain top. This could be related to the changes in the middle crust's density caused by volcanic activity.

The development of new approach, such as the DEXP transformation of gravity fields and their derivatives, can be used to estimate source depth without going through data filtering [Fedi, 2007]. The table below shows the comparison of gravity source depth values obtained by the DEXP method and spectral analysis for four locations in the study area.

Table 5. Comparison of gravity source depth values with previous authors at five study locations (points)

			De	epth (km)				
			Previous Studies					
X		This study	[Nnange et al., 2000]	[Evariste et al., 2014]	[<i>Marcel</i> et al., 2016]	[Kenfack et al., 2017]	D	
Χ	Y	Value based on DEXP Method	Value	based on S	Points	Location		
480	390	8	-	-	-	-	1	Bioko Island
520	460	7–12	7–9	4.5-7	8-12	4.73	3	Mount Cameroon
615	620	4–6	-	-	6–8	-	5	Manyemen and Fontem
520	460	8-10	_	_	6-8	_	2	Eséka

The depth estimate reveals the essence and relevance of the DEXP method when considered with the spectral analysis produced by previous authors.

Additionally, a deeper evaluation could be estimated in the region, but due to gaps in terrestrial gravity measurements that are not available in certain locations in the study area, our overall investigation was limited. For the region focused on Cameroon, the gravity database contains 61431 International Gravimetric Bureau (BGI) gravity anomalies (blue dots) and 745 (red dots) values from a specific campaign conducted by the NIC (National Institute of Cartography) of Cameroon from 2014 to 2017 [Barzaghi et al., 2021].

There were, however, big data gaps in remote locations; these gaps can be filled using Global Gravity Earth Models (GEMs) combining satellite, ground, and ocean data with XGM2019e. But the availability of terrestrial datasets found in these models for our study location is limited because no local campaigns were carried out in those areas. But the old models, like EGM 2008, didn't have the new gravity signal coming out of GOCE [Zingerle et al., 2020].

4.2. Geological Interpretation of Depth Estimates

The result obtained from the shallow depth estimate may be related to the short-wavelength bodies (shallow intrusive structures) in the region, which form parts of the volcanoes of the Cameroon Volcanic Line, as we can observe in the case of Bioko Island and Mt. Cameroon. Knowledge of the difference in depths from north to south of the CVL with large discrepancies may imply that the structures and volcanoes of the CVL are not continuous bodies. Meanwhile, there is a deeper source depth of more than 30 km aligning to the north of the CVL from Mount Bamboutos to Mount Oku. Such a large difference in anomalous bodies could either be a result of deep-seated igneous bodies found in the area.

The crust is thicker towards the north of the CVL along the Adamawa region compared to the southern part of Mt. Cameroon. A depth source of 4–6 kilometers around the Manyemen and Fontem areas and 8–10 kilometers in the Douala Basin (Eséka). This may have been caused by the large area and thick deposition of sedimentary formations in the upper crust.

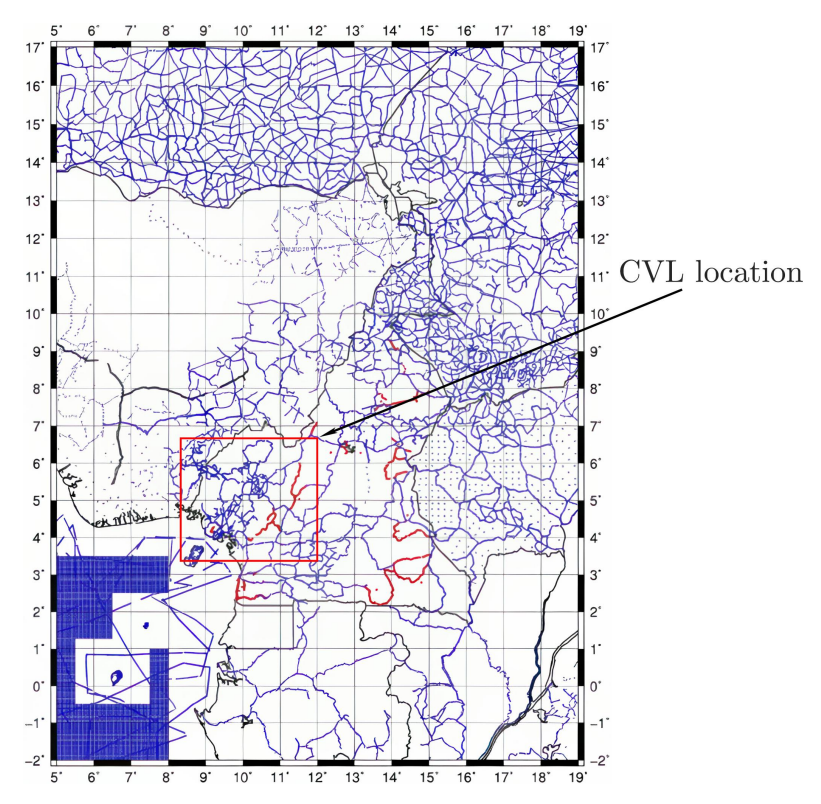


Figure 10. Database of gravity for geoid calculations in Cameroon and showing CVL location. Red dots: Terrestrial gravity measurements campaign, blue dots – BGI data [*Barzaghi et al.*, 2021].

4.3. Spectral Analysis Results

The spectral analysis for Moho depth estimates was calculated using the filtered gravity field separated from the DTU21 data that is not affected by topographic effects according to equation (1). The result of filtering can be seen in Figure 11.

Wiener filter theory, however, requires that the observed gravitational field be more or less stationary over the limits of the survey area [Pawlowski and Hansen, 1990]. This method is done using a Wiener filter that uses iterative steps to determine Moho depth, taking into account both lateral and radial changes in the crustal density of the Earth [Sampietro, 2015]. The estimates of filtered and unfiltered depth sources represent the mean depths of the whole study area. The spectral analysis curve was created from the power spectrum and the frequency domain of the separated field (Figure 12). The linear line segment of the slope corresponds to the mean depth of sources in the study area (CVL) of the separated field (Figure 12).

From the spectral analysis curve, we obtain that the mean deep source over the area represents 32.1 ± 6 km, while the shallow depth represents 6.7 ± 15 km. Some other parts of the spectrum represent noise data. The deep sources represent the Moho depth of the study area.

The Moho depth estimate of the study area was compared with the results of depth estimates done in the study area by other researchers. Both gravity and seismic methods (passive and Rayleigh waves) have been used for this comparison, as seen in Table 6.

Table 6. Moho depth estimate

DEXP depth (This study)	Moho depth from Spectral Analysis (This study)	Moho depth from Seismic [Tokam et al., 2010]	Moho depth from Gravity [Gallacher and Bastow, 2012]	Moho depth from Gravity [Goussi Ngalamo et al., 2018]	Moho depth from Gravity [Fairhead and Okereke, 1987]
30–40 km	$32.1 \pm 6 \text{km}$	$35.5 \pm 3.1 \text{ km}$	31.75 km	38.5 km	30–34 km

From these results, we conclude that Wiener filtration is an effective method to provide an accurate Moho depth estimate of the study area, which shows similar results to those obtained from previous studies. The result also ties in with the anomalous body found at a great depth of over 30 km towards the north of the 3D model. This also reveals that there are much deeper granitic intrusive bodies situated beneath the volcanoes along the CVL, particularly Mt. Bamboutos and Mt. Oku.

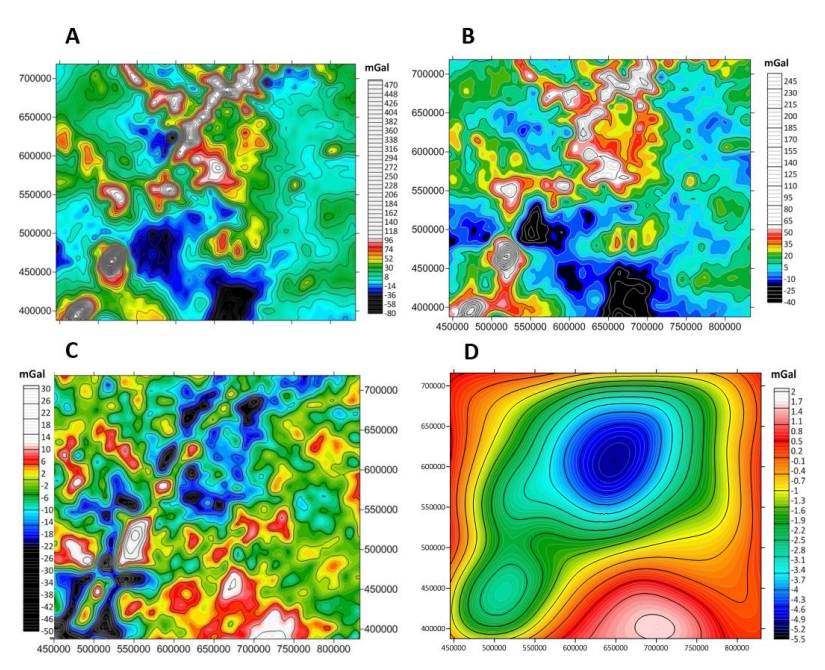


Figure 11. DTU21 gravity anomaly separation using wiener filter. A – Initial field at an altitude of 5 km B – Terrain-conditioned field, C – Field component not determined by relief, D – Field component not determined by relief at an altitude of 50 km.

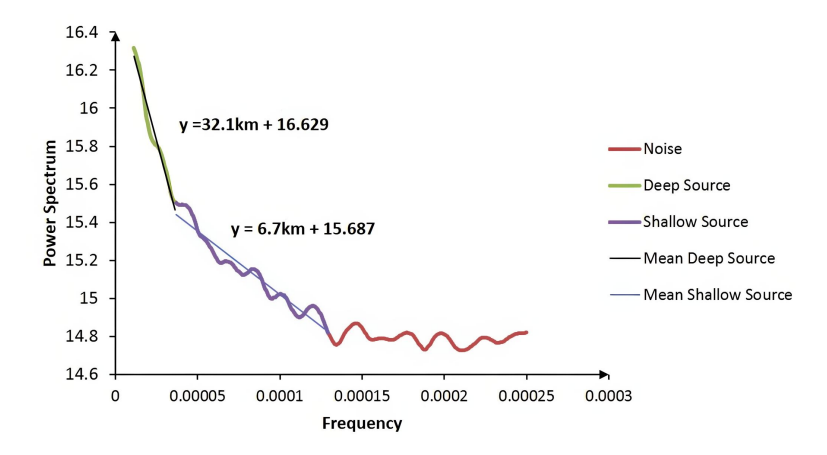


Figure 12. Spectral analysis curve for depth estimation.

5. Conclusion

The main focus of the research was to investigate the gravity source depth of CVL using DEXP as the main approach to illustrate its application in solving geophysical and geologic problems and revealing details of volcanic structures beneath the Earth's surface. Both DEXP and spectral analysis were carried out to complement the results and accuracy of the techniques.

We used the DEXP method to analyze results of depth along CVL that are in good agreement with previous geophysical findings. Our area of interest was successfully studied

using this method, but other disadvantages can be the gap in gravity data and the reliability of the method to completely display all gravity sources, both positive and negative, in the area. Since this is apparently a new approach, there is room for further improvement in the techniques for better results and evaluation. From DEXP, we could identify the following positive and negative gravity sources and depths (Table 7):

Table 7. Location of	potential g	gravity source	and their o	depths across	s the CVL

Location	Gravity anomalies	Depths (km)
Bioko Island	Positive	8
Mt. Cameroon	Positive	7–12
Manyemen and Fontem	Negative	4–6
Eséka	Negative	8–10

The research methods provided here are not common. Though they are new approaches to solving geological and geophysical problems, efforts can be made by other researchers to also apply the same techniques to study in more detail the features of CVL and its surroundings.

Acknowledgments. The current study was carried out in the Department of Geology and Geophysics Novosibirsk State University. I wish to thank all the collaborative support provided by the University and the Trofimuk Institute of Petroleum Geology and Geophysics for accepting this research.

References

Abate Essi, J. M., J. Marcel, J. Q. Yene Atangana, et al. (2017), Interpretation of gravity data derived from the Earth Gravitational Model EGM2008 in the Center-North Cameroon: structural and mining implications, *Arabian Journal of Geosciences*, 10(6), https://doi.org/10.1007/s12517-017-2919-y.

Abd-Elmotaal, H. A., K. Seitz, N. Kühtreiber, and B. Heck (2018), AFRGDB_V2.0: The Gravity Database for the Geoid Determination in Africa, in *International Symposium on Advancing Geodesy in a Changing World*, pp. 61–70, Springer International Publishing, Kobe, https://doi.org/10.1007/1345_2018_29.

Abdelrahman, E. M., S. Riad, E. Refai, and Y. Amin (1985), On the least-squares residual anomaly determination, *Geophysics*, 50(3), 473–480, https://doi.org/10.1190/1.1441925.

Aka, F. T., K. Nagao, M. Kusakabe, et al. (2004), Symmetrical Helium isotope distribution on the Cameroon Volcanic Line, West Africa, *Chemical Geology*, 203(3–4), 205–223, https://doi.org/10.1016/j.chemgeo.2003.10.003.

Apeh, O. I., and R. Tenzer (2022), Development of tailored gravity model based on global gravitational and topographic models and terrestrial gravity data for geophysical exploration of southern benue trough in southeast Nigeria, *Journal of Applied Geophysics*, 198, 104,561, https://doi.org/10.1016/j.jappgeo.2022.104561.

Barthelmes, F. (2013), Definition of functionals of the geopotential and their calculation from spherical harmonic models, *Scientific Technical Report*, https://doi.org/10.2312/GFZ.B103-0902-26.

Barzaghi, R., D. J. Carrion, L. H. Kamguia, et al. (2021), Estimating gravity field and quasi-geoid in Cameroon (CGM20), *Journal of African Earth Sciences*, 184, https://doi.org/10.1016/j.jafrearsci.2021.104377.

Begg, G. C., W. L. Griffin, L. M. Natapov, et al. (2009), The lithospheric architecture of Africa: Seismic tomography, mantle petrology, and tectonic evolution, *Geosphere*, 5(1), 23–50, https://doi.org/10.1130/GES00179.1.

Bloch, Y. I. (2009), Interpretation of gravitational and magnetic anomalies, 232 pp., Yu. I. Bloch (in Russian).

Burke, K. (2001), Origin of the Cameroon Line of Volcano-Capped Swells, *The Journal of Geology*, 109(3), 349–362, https://doi.org/10.1086/319977.

- Castaing, C., J. L. Feybesse, D. Thiéblemont, et al. (1994), Palaeogeographical reconstructions of the Pan-African/Brasiliano orogen: closure of an oceanic domain or intracontinental convergence between major blocks?, *Precambrian Research*, 69(1–4), 327–344, https://doi.org/10.1016/0301-9268(94)90095-7.
- Cheunteu Fantah, C. A., C. A. Mezoue, M. P. Mouzong, et al. (2022), Mapping of major tectonic lineaments across Cameroon using potential field data, *Earth, Planets and Space*, 74(1), https://doi.org/10.1186/s40623-022-01612-7.
- Déruelle, B., I. Ngounouno, and D. Demaiffe (2007), The 'Cameroon Hot Line' (CHL): A unique example of active alkaline intraplate structure in both oceanic and continental lithospheres, *Comptes Rendus. Géoscience*, 339(9), 589–600, https://doi.org/10.1016/j.crte.2007.07.007.
- Draper, N., and H. Smith (1998), *Applied Regression Analysis*, 709 pp., Wiley, https://doi.org/10.1002/9781118625590.
- Drewes, H., F. Kuglitsch, J. A. am, et al. (2016), The Geodesist's Handbook 2016, *Journal of Geodesy*, 90(10), 907–1205, https://doi.org/10.1007/s00190-016-0948-z.
- Dumont, J. F. (1986), Identification by remote sensing of the Sanaga accident (Cameroon). Its position in the context of the great accidents of Central Africa and the northern limit of the Congolese craton, *Geodynamics*, 1, 13–19 (in French).
- Elsheikh, A., S. Gao, and K. Liu (2014), Formation of the Cameroon Volcanic Line by lithospheric basal erosion: Insight from mantle seismic anisotropy, *Journal of African Earth Sciences*, 100, 96–108, https://doi.org/10.1016/j.jafrearsci.20 14.06.011.
- Esin, E. I., A. N. Vasilevskiy, and N. A. Bushenkova (2024), Spatial Correlations between the Terrain Features, Gravitational Field and Seismic Velocity Anomalies in the Central Kamchatka Region, *Russian Geology and Geophysics*, 65(2), 285–298, https://doi.org/10.2113/rgg20234579.
- Evariste, N. H., L. Genyou, T. C. Tabod, et al. (2014), Crustal structure beneath Cameroon from EGM2008, *Geodesy and Geodynamics*, 5(1), 1–10, https://doi.org/10.3724/sp.j.1246.2014.01001.
- Fairhead, J. D., and C. S. Okereke (1987), A regional gravity study of the West African rift system in Nigeria and Cameroon and its tectonic interpretation, *Tectonophysics*, 143(1–3), 141–159, https://doi.org/10.1016/0040-1951(87)90084-9.
- Fedi, M. (2007), DEXP: A fast method to determine the depth and the structural index of potential fields sources, *Geophysics*, 72(1), I1–I11, https://doi.org/10.1190/1.2399452.
- Fedi, M., and M. Pilkington (2011), Understanding imaging methods for potential field data, in *SEG Technical Program Expanded Abstracts* 2011, pp. 786–790, Society of Exploration Geophysicists, https://doi.org/10.1190/1.3628194.
- Fedi, M. G., and G. Florio (2013), Determination of the maximum-depth to potential field sources by a maximum structural index method, *Journal of Applied Geophysics*, 88, 154–160, https://doi.org/10.1016/j.jappgeo.2012.10.009.
- Förste, C., S. L. Bruinsma, O. Abrikosov, et al. (2014), EIGEN-6C4 The latest combined global gravity field model including GOCE data up to degree and order 2190 of GFZ Potsdam and GRGS Toulouse, https://doi.org/10.5880/ICGEM.2015.1.
- Gallacher, R. J., and I. D. Bastow (2012), The development of magmatism along the Cameroon Volcanic Line: Evidence from teleseismic receiver functions, *Tectonics*, *31*(3), https://doi.org/10.1029/2011tc003028.
- Gautier, K. P., L. Yap, Z. A. Alain, et al. (2021), Evaluation of global gravity field models using shipborne free-air gravity anomalies over the Gulf of Guinea, Central Africa, *Survey Review*, 54(384), 243–253, https://doi.org/10.1080/00396265.2021.1921519.
- Gautier Kamto, P., C. Mezoue Adiang, S. Nguiya, J. Kamguia, and L. Yap (2020), Refinement of Bouguer anomalies derived from the EGM2008 model, impact on gravimetric signatures in mountainous region: Case of Cameroon Volcanic Line, Central Africa, *Earth and Planetary Physics*, 4(6), 1–12, https://doi.org/10.26464/epp2020065.
- Gerard, A., and N. Debeglia (1975), Automatic Three-Dimensional Modeling for Interpretation of Gravity or Magnetic Anomalies, *Geophysics*, 40(6), 1014–1034, https://doi.org/10.1190/1.1440578.
- Ghomsi, F. E. K., N. R. Filho, R. Baldez, et al. (2021), Identification of Cameroon's geological structures through a gravity separation and using seismic crustal models, *Journal of African Earth Sciences*, 173, 104,027, https://doi.org/10.1016/j.jafrearsci.2020.104027.

- Gilardoni, M., M. Reguzzoni, and D. Sampietro (2016), GECO: a global gravity model by locally combining GOCE data and EGM2008, *Studia Geophysica et Geodaetica*, 60(2), 228–247, https://doi.org/10.1007/s11200-015-1114-4.
- Goussi Ngalamo, J. F., M. Sobh, D. Bisso, et al. (2018), Lithospheric structure beneath the Central Africa Orogenic Belt in Cameroon from the analysis of satellite gravity and passive seismic data, *Tectonophysics*, 745, 326–337, https://doi.org/10.1016/j.tecto.2018.08.015.
- Gruber, T., P. H. Zingerle, R. Pail, and X. Oikonomidou (2019), High resolution gravity field models as global reference surface for heights, SIRGAS.
- Kamgang, P., E. Njonfang, A. Nono, et al. (2010), Petrogenesis of a silicic magma system: Geochemical evidence from Bamenda Mountains, NW Cameroon, Cameroon Volcanic Line, *Journal of African Earth Sciences*, 58(2), 285–304, https://doi.org/10.1016/j.jafrearsci.2010.03.008.
- Kamguia, J., C. T. Tabod, R. Nouayou, et al. (2007), The Local Geoid Model of Cameroon: CGM05, Nordic Journal of Surveying and Real Estate Research, 4(2).
- Kamto, P. G., W. Lemotio, A.-P. K. Tokam, and L. Yap (2021), Combination of Terrestrial and Satellite Gravity Data for the Characterization of the Southwestern Coastal Region of Cameroon: Appraisal for Hydrocarbon Exploration, *International Journal of Geophysics*, 2021, 1–14, https://doi.org/10.1155/2021/5554528.
- Kenfack, J. V., J. M. Tadjou, J. Kamguia, et al. (2011), Gravity Interpretation of the Cameroon Mountain (West Central Africa) Based on the New and Existing Data, *International Journal of Geosciences*, 02(04), 513–522, https://doi.org/10.4236/ijg.2011.24054.
- Kenfack, J. V., J. Kamguia, K. D. Armand, et al. (2017), Estimation of the Depth of Major Subsurface Discontinuities Beneath the Mount Cameroon Region, Central Africa, Based on New and Existing Gravity Data Analysis, *Earth Science Research*, 6(1), 142, https://doi.org/10.5539/esr.v6n1p142.
- Kokoshkin, A. V., V. A. Korotkov, K. V. Korotkov, et al. (2015), Universal reference spectrum use for noise-to-signal ratio estimation in the Wiener filter, *Zhurnal Radioelektroniki*, (7) (in Russian).
- Lawrence, S., S. Munday, and R. Bray (2002), Regional geology and geophysics of the eastern Gulf of Guinea (Niger Delta to Rio Muni), *The Leading Edge*, 21(11), 1112–1117, https://doi.org/10.1190/1.1523752.
- Lee, J., and J. H. Kwon (2020), Precision Evaluation of Recent Global Geopotential Models based on GNSS/Leveling Data on Unified Control Points, *Journal of the Korean Society of Surveying, Geodesy, Photogrammetry and Cartography*, 38(2), 153–163, https://doi.org/10.7848/ksgpc.2020.38.2.153.
- Marcel, J., N. P. Njandjock, C. T. Tabob, and E. Manguelle-Dicoum (2010), Moho Depth Estimates for the Cameroon Volcanic Line from Gravity Data, *International Journal of Economic and Environmental Geology*, 1, 17–20.
- Marcel, J., J. M. Abate Essi, P. N. Nouck, et al. (2016), Structure of the Crust Beneath the South Western Cameroon, from Gravity Data Analysis, *International Journal of Geosciences*, 07(08), 991–1008, https://doi.org/10.4236/ijg.2016.78075.
- Marcel, J., J. M. Abate Essi, P. N. Nouck, et al. (2018), Validation of gravity data from the geopotential field model for subsurface investigation of the Cameroon Volcanic Line (Western Africa), *Earth, Planets and Space*, 70(1), https://doi.org/10.1186/s40623-018-0812-x.
- Matheron, G. (1963), Principles of geostatistics, *Economic Geology*, 58(8), 1246–1266, https://doi.org/10.2113/gsecongeo. 58.8.1246.
- Moundi, A., P. Wandji, J.-M. Bardintzeff, et al. (2007), Les basaltes éocènes à affinité transitionnelle du plateau Bamoun, témoins d'un réservoir mantellique enrichi sous la ligne volcanique du Cameroun, *Comptes Rendus. Géoscience*, 339(6), 396–406, https://doi.org/10.1016/j.crte.2007.04.001 (in French).
- Murthy, I. V. R., and S. K. G. Krishnamacharyulu (1990), Polyfit: A Fortran 77 Program to Fit a Polynomial of Any Order to Potential Field Anomalies, *Journal of Association of Exploration Geophysicists*, 11, 99–105.
- Ndikum, E. N., C. T. Tabod, B. Z. Essimbi, et al. (2014), Gravity Model for an Anomalous Body Located in the NW Portion of the Douala Sedimentary Sub-Basin, Cameroon (Central Africa), *Open Journal of Geology*, 04(10), 524–541, https://doi.org/10.4236/ojg.2014.410039.

- Nguiya, S., M. M. Pemi, A. K. Tokam, et al. (2019), Crustal structure beneath the Mount Cameroon region derived from recent gravity measurements, *Comptes Rendus*. *Géoscience*, 351(6), 430–440, https://doi.org/10.1016/j.crte.2019.05.001.
- Njandjock, N. P., E. Manguelle-Dicoum, M. T. Ndougsa, and C. T. Tabod (2006), Spectral analysis and gravity modelling in the Yagoua, Cameroon, sedimentary basin, *Geofísica Internacional*, 45(3), 209–215, https://doi.org/10.22201/igeof. 00167169p.2006.45.3.206.
- Njeudjang, K., J. M. Abate Essi, J. D. Kana, et al. (2020), Gravity investigation of the Cameroon Volcanic Line in Adamawa region: Geothermal features and structural control, *Journal of African Earth Sciences*, 165, 103,809, https://doi.org/10.1016/j.jafrearsci.2020.103809.
- Njome, M. S., and M. J. de Wit (2014), The Cameroon Line: Analysis of an intraplate magmatic province transecting both oceanic and continental lithospheres: Constraints, controversies and models, *Earth-Science Reviews*, 139, 168–194, https://doi.org/10.1016/j.earscirev.2014.09.003.
- Nnange, J., V. Ngako, J. Fairhead, and C. Ebinger (2000), Depths to density discontinuities beneath the Adamawa Plateau region, Central Africa, from spectral analyses of new and existing gravity data, *Journal of African Earth Sciences*, 30(4), 887–901, https://doi.org/10.1016/s0899-5362(00)00058-0.
- Noel, E., M. Marcelin, and A. Bekoa (2014), Crustal Structure and Seismogenic Zone of Cameroon: Integrated Seismic, Geological and Geophysical Data, *Open Journal of Earthquake Research*, 03(04), 152–161, https://doi.org/10.4236/ojer. 2014.34015.
- Pavlis, N. K., S. A. Holmes, S. C. Kenyon, and J. K. Factor (2012), The development and evaluation of the Earth Gravitational Model 2008 (EGM2008), *Journal of Geophysical Research: Solid Earth*, 117(B4), https://doi.org/10.1029/2011jb008916.
- Pawlowski, R. S., and R. O. Hansen (1990), Gravity anomaly separation by Wiener filtering, *Geophysics*, 55(5), 539–548, https://doi.org/10.1190/1.1442865.
- Sampietro, D. (2015), Geological units and Moho depth determination in the Western Balkans exploiting GOCE data, *Geophysical Journal International*, 202(2), 1054–1063, https://doi.org/10.1093/gji/ggv212.
- Spector, A., and F. S. Grant (1970), Statistical Models for Interpreting Aeromagnetic Data, *Geophysics*, 35(2), 293–302, https://doi.org/10.1190/1.1440092.
- Suh, C. E., S. N. Ayonghe, R. S. J. Sparks, et al. (2003), The 1999 and 2000 eruptions of Mount Cameroon: eruption behaviour and petrochemistry of lava, *Bulletin of Volcanology*, 65(4), 267–281, https://doi.org/10.1007/s00445-002-0257-7.
- Tokam, A.-P. K., C. T. Tabod, A. A. Nyblade, et al. (2010), Structure of the crust beneath Cameroon, West Africa, from the joint inversion of Rayleigh wave group velocities and receiver functions: Joint inversion in Cameroon, *Geophysical Journal International*, 183(2), 1061–1076, https://doi.org/10.1111/j.1365-246x.2010.04776.x.
- Toteu, S. F., J. Penaye, and Y. P. Djomani (2004), Geodynamic evolution of the Pan-African belt in central Africa with special reference to Cameroon, *Canadian Journal of Earth Sciences*, 41(1), 73–85, https://doi.org/10.1139/e03-079.
- Yokoyama, T., F. T. Aka, M. Kusakabe, and E. Nakamura (2007), Plume-lithosphere interaction beneath Mt. Cameroon volcano, West Africa: Constraints from 238U-230Th-226Ra and Sr-Nd-Pb isotope systematics, *Geochimica et Cosmochimica Acta*, 71(7), 1835–1854, https://doi.org/10.1016/j.gca.2007.01.010.
- Zhou, R., and X. Wu (2015), An iterative Wiener filtering method based on the gravity gradient invariants, *Geodesy and Geodynamics*, 6(4), 286–291, https://doi.org/10.1016/j.geog.2015.06.002.
- Zingerle, P., R. Pail, T. Gruber, and X. Oikonomidou (2019), *The experimental gravity field model XGM2019e*, GFZ Data Services, https://doi.org/10.5880/ICGEM.2019.007.
- Zingerle, P., R. Pail, T. Gruber, and X. Oikonomidou (2020), The combined global gravity field model XGM2019e, *Journal of Geodesy*, 94(7), https://doi.org/10.1007/s00190-020-01398-0.